AIMS Materials Science, 10(5): 909–933.
DOI: 10.3934/matersci.2023049
Received: 22 June 2023
Revised: 21 September 2023
Accepted: 08 October 2023
Published: 24 October 2023

http://www.aimspress.com/journal/Materials

Review

Cu-based mutlinary sulfide nanomaterials for photocatalytic applications

Liang Wu*

School of Chemistry and Materials Science, Anhui Normal University, Wuhu 241002, China

* **Correspondence:** Email: wuliang@ahnu.edu.cn.

Abstract: Due to their environmentally benign elemental components, suitable bandgap and high absorption coefficient in the visible-light range, Cu-based multinary sulfides exhibit excellent photocatalytic properties. Moreover, the adjustable atomic structure and unique electronic state of Cu-based multinary sulfide semiconductors can boost their ability to absorb visible light. In this review, we provide a summary of recent progress in photocatalytic applications of Cu-based multinary sulfide nanomaterials, including Cu-based ternary sulfides ($CuInS_2$, $CuIn_5S_8$, Cu_3SnS_4, $CuFeS_2$, etc.) and Cu-based quaternary sulfides (CuZnInS, Cu_2ZnSnS_4, CuZnGaS, CuInGaS, etc.). We start with a review of the bandgap alignments of Cu-based ternary sulfides and Cu-based quaternary sulfides, which are the key factors for the photocatalytic activity of semiconductor photocatalysts. Then, we discuss the advancements in photocatalytic applications of Cu-based multinary sulfide photocatalysts, including photocatalytic H_2 production, CO_2 reduction, organic synthesis and degradation of pollutants and photoelectrochemical H_2 production. Finally, we end this review with a summary of the current challenges and opportunities of Cu-based multinary sulfides in future studies.

Keywords: Cu-based multinary sulfide nanomaterials; photocatalytic H_2 production; photoelectrochemical H_2 production; photocatalytic CO_2 reduction; photocatalytic organic synthesis; photocatalytic pollutant removal

1. Introduction

The demand for energy is increasing with the development of industrialization and information technology. Otherwise, the use of fossil fuels will emit a large amount of carbon dioxide and give rise to environmental pollution. Therefore, how to use new technology and materials to solve the increasingly

tense energy crisis and severe environmental problems has become a hot spot in material and chemistry research fields. Solar energy is the most abundant and clean green energy.

Photocatalysis using solar energy is an appealing technology to address the energy crisis and environmental problems [1–5]. The photocatalytic reaction is generally divided into three steps. (I) Photocatalysts absorb light to produce both excited holes and electrons. (II) The holes and electrons transfer to the surface of the photocatalyst. (III) The surface carriers participate in the redox reaction [6]. Specifically, semiconductor photocatalysts stir up the electrons in the valance band (VB) to the conduction band (CB) to produce hole-electron pairs [7–9]. Subsequently, the photogenerated carriers are separated and diffused from the bulk to the surface of the photocatalyst. Obviously, the light absorption efficiency, the charge separation and diffusion efficiency and the redox reaction efficiency are the three key parameters for determining the conversion efficiency of the photocatalytic reaction [10–13]. Therefore, the most important issue in photocatalysis is designing photocatalysts from the above three aspects to achieve high conversion efficiency.

Semiconductor nanomaterials have attracted extensive attentions due to the special properties stemming from the quantum effect [14–16]. As the size is less than the exciton Bohr radius, the electron density of the semiconductor nanomaterials will be discontinuous, and the carrier will have a spatial limiting effect and cause a change in the band structure [17–19]. On the other hand, the huge surface area of semiconductor nanomaterials will bring ignored surface effects. The tunable bandgaps and special surface effect of semiconductor nanomaterials will bring novel optical and electronic properties, rendering them as promising candidates for photocatalytic applications [20–22].

To date, a series of semiconductor nanomaterials have been developed as photocatalysts, such as metal oxides (TiO_2, ZnO, WO_3, etc.), metal chalcogenides (CdS, CdSe, etc.) and polymers [23–29]. Among the most widely investigated semiconductor photocatalysts, Cu-based multinary sulfide (CMS) nanomaterials have attracted wide interest in various photocatalytic applications due to their suitable and tunable bandgap, high absorption coefficient, environmental benign elemental components, unique electronic state and adjustable atomic structure [30–34]. CMSs are inorganic compounds consisting of at least two metal elements. The band structure of these CMSs can be conveniently adjusted through metal element alloying, then optimizing their photocatalytic performances [35–38]. The diversity of metal elements in CMSs will bring different crystal structures and allow precise control of the reactive atomic arrangement on the surface to construct specific active sites for diversified photocatalytic reactions [39–42]. At the same time, the differential charge distribution of diverse elements will result in microcosmic polarization and lead to a built-in electric field, which is beneficial for the effective separation of photogenerated holes and electrons [43,44]. Due to these specialties, CMS nanomaterials exhibit excellent performance in photocatalytic H_2 production, CO_2 reduction, organic synthesis, photoelectrochemical (PEC) H_2 production, and so on [45–49].

In this review, we provide a comprehensive overview on recent research of CMS nanomaterials in photocatalytic applications. We focus on the most researched CMSs, namely Cu-based ternary and quaternary sulfide nanomaterials. We first introduce the bandgap alignments of Cu-based ternary sulfides ($CuInS_2$, $CuIn_5S_8$, Cu_3SnS_4, etc.) and Cu-based quaternary sulfides (CuZnInS, Cu_2ZnSnS_4, CuInGaS, etc.), which are the key factors for the photocatalytic activity of semiconductor photocatalysts. Subsequently, we provide a summary of recent progress in the photocatalytic applications of Cu-based ternary sulfides and Cu-based quaternary sulfide nanomaterials, focusing on photocatalytic H_2 production, CO_2 reduction, organic synthesis, degradation of pollutants and PEC H_2

production. Finally, we also summarize the current challenges and opportunities of Cu-based multinary sulfides in future studies.

2. Cu-based multinary sulfide nanomaterials

To date, the developed CMS nanomaterials mainly focused on Cu-based ternary and quaternary sulfides (Figure 1). This section will introduce the bandgap alignments of Cu-based ternary ($CuInS_2$, $CuIn_5S_8$, Cu_3SnS_4, $CuFeS_2$, etc.) and quaternary sulfides (CuZnInS, Cu_2ZnSnS_4, CuZnGaS, CuInGaS, etc.) in detail.

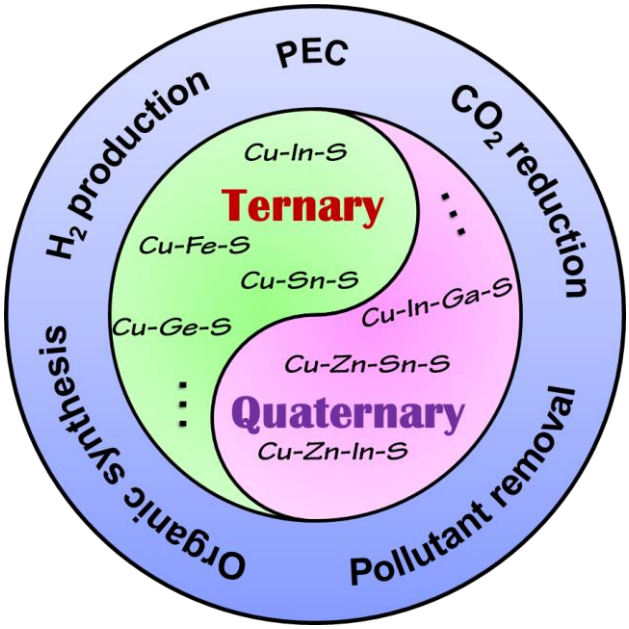

Figure 1. Schematic illustration of the photocatalytic applications of Cu-based ternary and quaternary sulfide nanomaterials.

2.1. Cu-based ternary sulfide nanomaterials

Cu-based ternary sulfides are ZnS-derived compounds produced by replacing Zn atoms with Cu cations and trivalent/tetravalent cations (e.g., In, Ga, Sn, Ge, Fe, etc.) [50,51]. Cu-III-S compounds (III = In, Ga) preferentially crystallize in a diamond-like structure inherited from ZnS. For example, the stoichiometric formula $CuInS_2$ (CIS) exhibits a stable chalcopyrite structure at room temperature and a metastable wurtzite structure at high temperature [52]. The tolerance of cation off-stoichiometry allows Cu-III-S chalcopyrite compounds to introduce different cation ratios, producing nonstoichiometric ternary sulfides, such as $CuIn_3S_5$, $CuIn_5S_8$, and $CuIn_{11}S_{17}$ [53,54]. Moreover, the off-stoichiometry effect usually has great influences on the band structures, optical properties and crystal structures of Cu-III-S compounds. The bandgaps of $CuInS_2$ and $CuIn_5S_8$ are 1.5 and 2.06 eV, respectively [55,56]. In addition, the VB and CB positions of $CuInS_2$ are also different from these of $CuIn_5S_8$ (Figure 2). The bandgap will change from 1.5 to 2.35 eV when the In cation is replaced by a Ga cation (Figure 2) [57].

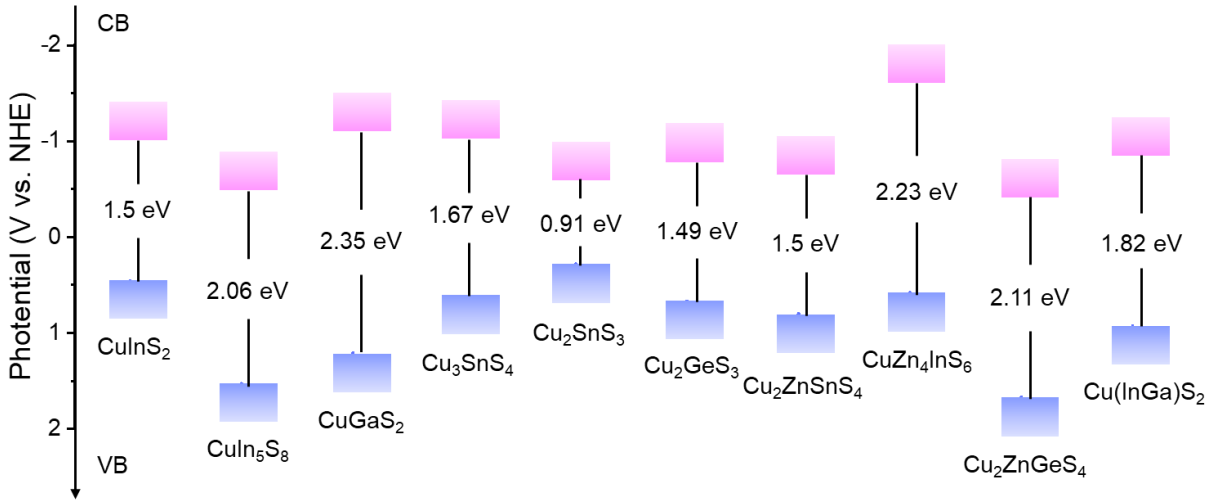

Figure 2. Band position of representative Cu-based ternary and quaternary sulfide semiconductors.

The most reported Cu-IV-S compounds are stoichiometry Cu_2SnS_3 (CTS) and Cu_2GeS_3, which generally crystallize in zinc-blende, orthorhombic and wurtzite structures [58,59]. Similar to Cu-In-S compounds, tolerating cation off-stoichiometry usually leads to nonstoichiometric ternary sulfides, such as, Cu_3SnS_4, Cu_4SnS_4, and $Cu_2Sn_3S_7$ [60,61]. The different cation ratios will lead to different bandgap alignments of Cu-Sn-S compounds. For example, the bandgaps of Cu_2SnS_3 and Cu_3SnS_4 are 0.91 and 1.67 eV, respectively, and possess different VB and CB positions (Figure 2) [62,63]. Cu_2GeS_3 with a monoclinic structure has a bandgap of 1.49 eV (Figure 2) [34]. In addition to the above Cu-IV-S compounds, $CuFeS_2$ (CFS), obtained by replacing Zn atoms with Cu cations and Fe cations, is another well-studied ternary sulfide [64–66]. The special band structures and high visible-light absorption efficiency favor the utilization of Cu-based ternary sulfides in photocatalytic H_2 production, CO_2 reduction, organic synthesis and pollutant removal.

2.2. Cu-based quaternary sulfide nanomaterials

Cu-based quaternary sulfides have attracted extensive research interests in photocatalytic applications as fascinating and promising nanomaterials. Many types of Cu-based quaternary sulfides have been designed and synthesized via regulation of metal types and ratios, such as Cu-II-VI-S compounds obtained via successive replacement of the In atoms in $CuInS_2$ with II and VI atoms obeying the octet rule [44], and Cu-II-V-S compounds obtained via partially replacing of the In atoms in $CuInS_2$ with II atoms [35,67]. As far back as 1950, scientists designed quaternary chalcogenide via cation substitution [68]. A series of Cu-based quaternary sulfides have been synthesized for photocatalytic applications in recent decades, such as Cu_2ZnSnS_4 (CZTS), CuZnInS (CZIS), Cu_2CdSnS_4 (CCTS), Cu_2ZnGeS_4 (CZGS), and CuGaInS (CGIS) [69–73]. As the most researched quaternary chalcogenide, CZTS is an n-type semiconductor with a bandgap of 1.5 eV [31], which can absorb all visible light for photocatalytic applications. In addition, the other Cu-based quaternary sulfides also have suitable bandgaps for visible-light absorption, namely $CuZn_4InS_6$ with a bandgap of 2.23 eV, CZGS with a bandgap of 2.11 eV and CGIS with a bandgap of 1.82 eV (Figure 2) [39,40,74,75]. Due to their special band structures, high visible-light absorption efficiency and tunable surface atomic

arrangements, Cu-based quaternary sulfides are widely used for photocatalytic H_2 production, organic synthesis, degradation of pollutants and PEC H_2 evolution.

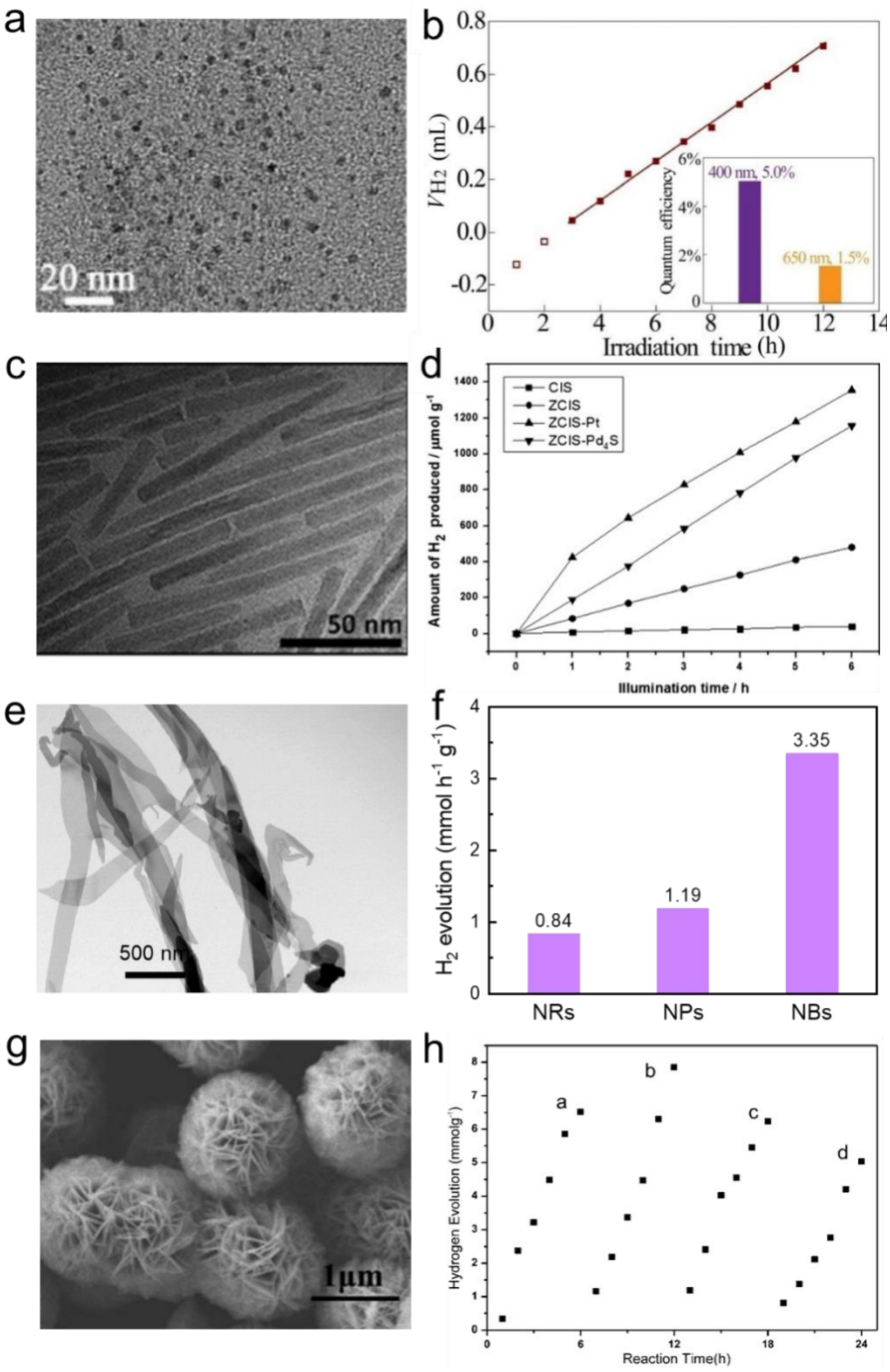

Figure 3. (a, b) Transmission electron microscope (TEM) image and photocatalytic H_2 evolution properties of 0D CZIS nanocrystals (Reproduced from Ref. [76] with permission). (c, d) TEM image and photocatalytic H_2 evolution properties of 1D CZIS nanorods (Reproduced from Ref. [77] with permission). (e, f) TEM image and photocatalytic H_2 evolution properties of 2D CZIS nanobelts [40]. (g, h) Scanning electron microscope (SEM) image and photocatalytic H_2 evolution properties of 3D Cu_3SnS_4 flower-like microspheres (Reproduced from Ref. [78] with permission).

3. Photocatalytic applications of Cu-based multinary sulfide nanomaterials

3.1. Photocatalytic H_2 production

Hydrogen energy is a kind of secondary energy with abundant sources and wide applications. However, almost no elementary hydrogen exists on Earth. Hydrogen can be produced by the decomposition of hydrogen-containing materials. Water is the most abundant hydrogen-containing compound on Earth, so water splitting is an efficient and sustainable method for hydrogen production. Photocatalytic hydrogen production is a green and sustainable hydrogen production program. In photocatalytic overall water splitting, water molecules are split into hydrogen and oxygen on the surface of photocatalysts under irradiation [8,79,80].

To date, various kinds of CMSs have been used for solar-to-hydrogen production. Kudo and coauthors first used CZIS powder for photocatalytic H_2 evolution from aqueous solutions containing K_2SO_3 and K_2S under visible-light irradiation [67]. With the development of nanotechnology, CMS nanomaterials have been designed and synthesized for solar-driven hydrogen production [81–84]. For example, Wu and coauthors reported the synthesis of CIS quantum dots (QDs) via an aqueous synthetic approach, which exhibited excellent photocatalytic hydrogen evolution performances [84]. Ning and coauthors successfully prepared water soluble CZIS QDs for photocatalytic hydrogen production (Figure 3). The CIZS QDs passivated by glutathione ligands are highly stable in aqueous conditions (Figure 3a) and show significant energy conversion efficiency in the visible and near-infrared regions with an external quantum efficiency (EQE) of ~1.5% at 650 nm (Figure 3b), which is the highest EQE reported in the near-infrared region [76]. In addition, many strategies have been used to improve the photocatalytic hydrogen production performances of CMS QDs. For instant, Pt and Au co-catalysts have been loaded on the surface of CZTS nanocrystals to significantly improve the photocatalytic H_2 evolution performances [31,82,85,86]. Heterojunctions and homojunctions are designed in CZTS to promote the separation of photogenerated charges and then optimize their photocatalytic performances [43,87–89].

One-dimensional (1D) nanostructures exhibit novel physicochemical properties brought about by changes in dimension, size and composition [90–92]. In particular, the continuity of charge transport brings out the unique advantages of 1D materials in photocatalytic and photoelectronic applications. Various types of 1D semiconductor nanomaterials have been developed for photocatalytic hydrogen production [26,93,94]. Han and coauthors have successfully synthesized wurtzite CZIS nanorods using a one-pot non-injection method for solar-to-hydrogen production (Figure 3c) [32,77]. Subsequently, Pt and Pd_4S nanoparticles were decorated on the tips of CZIS nanorods to improve their photocatalytic performances. The Pt and Pd_4S cocatalysts can accelerate charge separation and act as active sites for hydrogen production, resulting in remarkably improved photocatalytic performance (Figure 3d). Low-cost and noble-metal-free 1D CZTS nanofibers also exhibit excellent photocatalytic hydrogen production performance under visible-light irradiation [95].

Due to the solo ability of confinement of electrons in their layer, two-dimensional (2D) nanomaterials possess special optical and electronic properties. In addition, 2D semiconductor nanomaterials can reduce the recombination rate and shorten the migration distance of photogenerated carriers. The layered structure facilitates the light absorption process even at low flux density, and the photogenerated carriers are only required to transfer a very small distance. Moreover, the large surface area of 2D nanomaterials favors surface reactions. Thus, 2D semiconductor nanomaterials are widely

used for solar-to-hydrogen production [96–99]. Wang and coauthor first reported the synthesis of graphene-like CZTS nanosheets using a facile template-free approach [100]. The synthesized CZTS nanosheets with a thickness of ca. 2–3 nm exhibited high activity and stability for solar-to-hydrogen production without loading cocatalysts. Note that the 2D structure can expose the highest active facet. We first used first-principle-density functional theory calculations to explore the reaction Gibbs energy (ΔG_H) of the (0001), (1010) and (1011) facets of wurtzite CZIS, finding that the (0001) facet has the smallest binding strength to atomic hydrogen. We then designed a simple colloidal method to synthesize single crystalline wurtzite CZIS nanobelts (NBs) exposing the (0001) facet assisted with oleylamine and 1-dodecanethiol (Figure 3e). The synthesized CZIS nanobelt photocatalysts show excellent photocatalytic performances under visible-light irradiation without cocatalyst (Figure 3f) [40]. Furthermore, we doped phosphorus into 2D single crystalline CZIS sulfide nanobelts to reduce the recombination rate and increase the electric conductivity of photogenerated carriers, enabling significantly improved photocatalytic H_2 evolution performance [39].

In addition, three-dimensional (3D) CMSs have also been developed as photocatalysts for solar-to-hydrogen production. Xie and coauthors have constructed monodisperse CIS hierarchical microarchitectures for photocatalytic hydrogen production [101]. The obtained monodisperse CIS hierarchical photocatalyst showed an average hydrogen production rate of 59.4 μmol h^{-1} g^{-1} under visible light irradiation. Qian and coauthors successfully synthesized 3D-hierarchical Cu_3SnS_4 flower-like microspheres via a solvothermal process (Figure 3g) [78]. The bandgap of the obtained Cu_3SnS_4 microspheres is 1.38 eV, which is suitable for UV and near-IR light absorption. The 3D Cu_3SnS_4 photocatalysts without cocatalyst show good photocatalytic activity with a H_2 evolution rate of 1.1 mmol h^{-1} g^{-1} (Figure 3h). 3D Cu-based quaternary sulfides also exhibit excellent photocatalytic hydrogen production performances, such as CZIS hollow microspheres and hollow sub-microspheres [102,103].

3.2. Photoelectrochemical H_2 evolution

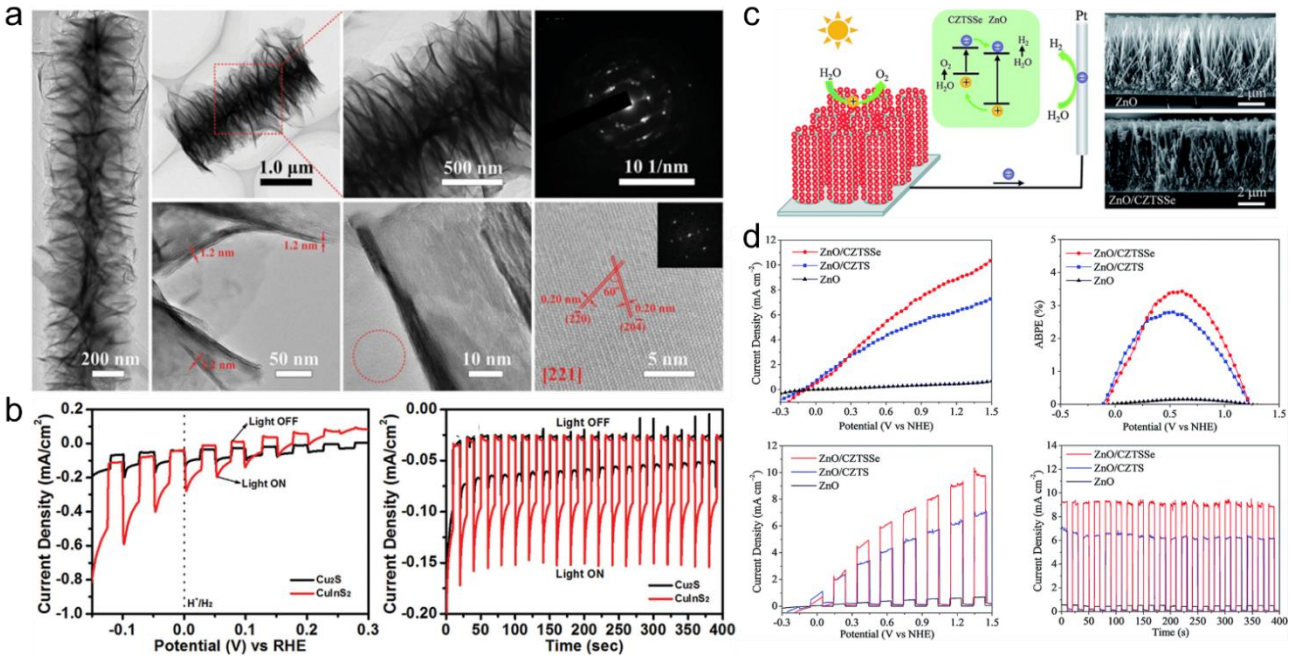

Figure 4. (a) TEM, selected area electron diffraction (SAED) and high-resolution TEM (HRTEM) images of CIS nanosheet-constructed nanowires. (b) Linear sweep voltammetry (LSV) curves and intensity-time (I-t) curves (at 0 V versus reversible hydrogen electrode (RHE)) of the pristine Cu_2S nanowire arrays and CIS nanosheet-constructed nanowire arrays under simulated solar illumination (Reproduced from Ref. [104] with permission). (c) A schematic and SEM images of the ZnO/CZTS photoanode. (d) LSV, ABPE, chopped LSV and I-t (at 1.23 V versus RHE) curves of the three photoanodes of ZnO/CZTSSe, ZnO/CZTS and ZnO (Reproduced from Ref. [105] with permission).

Photoelectrochemical water splitting provides a promising strategy to convert solar energy into hydrogen [106–108]. Previously, many common photovoltaic materials such as CdTe, TiO_2 and Si were successfully used to fabricate photoelectrodes for PEC solar water splitting and obtained significant results [109–111]. However, the toxicity of Cd in CdTe, the narrow light absorption range and the high energy fabrication process of Si limited their large-scale applications in PEC water splitting. Thus, scientists are searching for high-efficiency, low-cost and wide light absorption materials for PEC applications. Copper-based multinary chalcogenides such as CIS, $Cu(InGa)Se_2$ (CIGSe), and CZTS have been used as potential photocathode materials due to their excellent photovoltaic performances and suitable conduction band positions for water reduction [48,112–117]. For example, the CIGSe/CdS/ZnO photocathode exhibited excellent PEC performance with a current upping to 32.5 mA cm^{-2} at 0 V_{RHE} [118]. Then, CMS nanomaterials were also used to fabricate photoelectrodes for PEC applications with the development of nanotechnology [119–121].

Guo and coauthors fabricated CZTS photoelectrode using colloidal CZTS nanocrystals via electrophoretic deposition. The obtained CZTS photoelectrode exhibited composition-dependent PEC hydrogen production performances [122]. The $(Cu_2Sn)_{0.45}Zn_{1.65}S_3$ photocathode has the highest photocurrent with an incident photon to current conversion efficiency (IPCE) of 3.9% at 600 nm, which

is higher than previously reported results of CZTS photocathodes [123]. Similarly, the CZIS photoelectrode fabricated by 2D CZIS nanoplates also showed a cathodic photocurrent [124]. Moon and coauthors synthesized chalcopyrite CIS nanorod arrays as photoelectrodes for PEC hydrogen production via anodic aluminum oxide template-assisted growth. The CIS nanorod arrays showed an obvious cathodic photocurrent response without co-catalyst loading [125]. Zhang and coauthors reported the synthesis of chalcopyrite CIS nanosheet-constructed nanowire arrays (NCNAs) (Figure 4a). The PEC properties of these NCNAs were investigated using a three-electrode system with a reference electrode of Ag/AgCl and counter electrode of a Pt mesh in a 1.0 M KCl aqueous solution. The CIS NCNA photocathode exhibited not only enhanced PEC performance, but also improved PEC stability (Figure 4b) [104]. Many strategies have been developed to improve the PEC performances of CMS photoelectrodes. For example, Sivula and coauthors used CdS, ZnSe and CdSe buffer layers to modify the surface of CZTS nanocrystal photocathodes to enhance the PEC performance [126]. Pradhan and coauthors integrated Au on CIS nanocrystals to improve the PEC performance of CIS nanoplates [127]. The exciton–plasmon coupling in the 0D–2D dot–disk Au-CIS heterostructures leads to a higher photocurrent with efficient production of H_2.

Among the widely used PEC materials, some wide-bandgap metal oxides (such as ZnO and TiO_2) are promising stable, efficient and inexpensive anode materials for efficient PEC hydrogen production [128,129]. However, the large bandgaps of metal oxides limit the absorption of visible light, thus reducing the solar-to-hydrogen conversion efficiency. Sensitization using QDs, especially CMS CDs, is one of the most promising strategies to expand the light absorption range of metal oxides, mainly due to the suitable bandgap of CMS QDs [130–133]. Teng and coauthors used colloidal CIS CDs as sensitizers for TiO_2 photoelectrodes [134]. The CIS-sensitized TiO_2 photoelectrodes exhibited a maximum conversion efficiency of 1.9% at +0.23 V bias. Wang and coauthors used CZIS CDs to sensitize TiO_2 photoelectrodes. The obtained CZIS/TiO_2 photoelectrodes showed composition-dependent performances with a maximum photocurrent density of 3.7 mA cm^{-2} [135]. In addition, 2D CZIS nanosheet-sensitized TiO_2 nanorods can also boost their solar water splitting performance [136]. Xu and coauthors studied the PEC performance of CZTS-sensitized ZnO nanorod photoanodes in detail. CZTS/ZnO photoanodes are fabricated by spin-coating CZTS nanocrystals on ZnO arrays (Figure 4c). The ZnO/CZTSSe photoelectrode showed excellent PEC performances with a photocurrent density of 6.38 mA cm^{-2} at 1.23 V_{RHE} and an optimal applied bias photon-to-current efficiency (ABPE) of 2.8% at a bias of 0.60 V (Figure 4d) [105].

3.3. Photocatalytic CO_2 reduction

Excessive CO_2 emissions have led to greenhouse effects and several serious environmental problems. Converting CO_2 into hydrocarbon fuels is a promising approach to lower the CO_2 concentration in the atmosphere and can also reduce the dependence on fossil fuels. Inspired by the photosynthesis of plants, photocatalytic CO_2 reduction to hydrocarbon fuels using solar energy is an attractive method for CO_2 conversion and can mitigate greenhouse gas emissions. A series of photocatalysts have been explored for photocatalytic CO_2 reduction, such as metal oxides, metal nitrides, and metal sulfides [137–140]. Among them, metal sulfides are excellent catalysts for photocatalytic or PEC CO_2 reduction because the S 3p orbital occupies the less positive VB, which promote metal sulfides with a wider photoresponse range and higher carrier concentration, and sulfur

has light-effective mass carriers [141,142]. CMS semiconductors with a narrow bandgap and excellent light absorption abilities have been widely studied for photocatalytic and PEC CO_2 reduction [143–146].

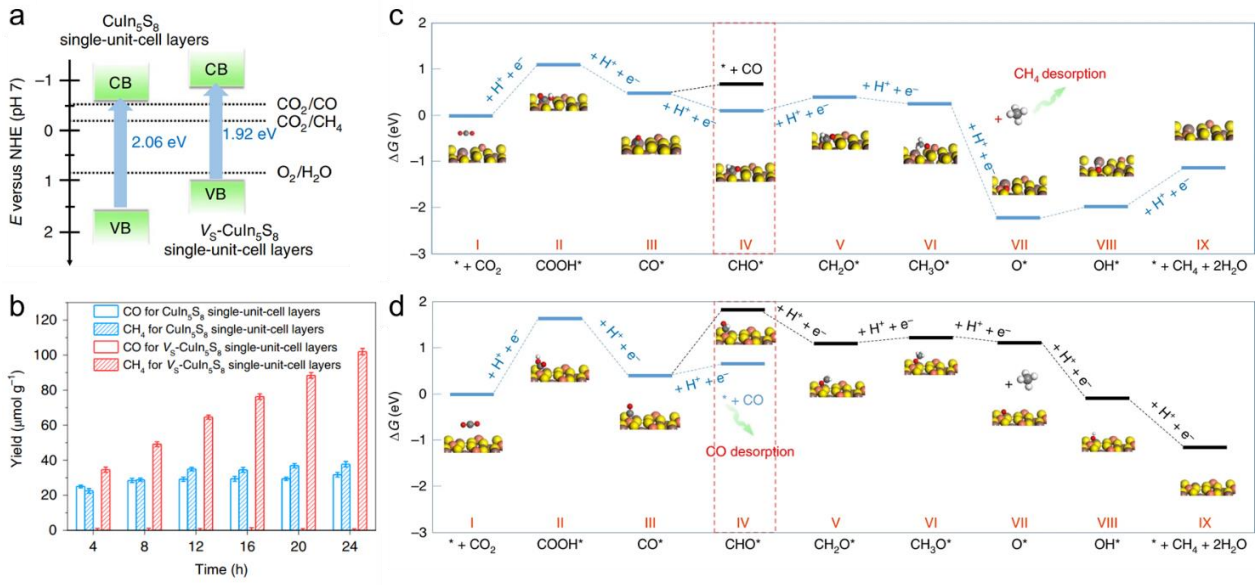

Figure 5. (a) Bandgap alignments of $CuIn_5S_8$ and Vs-$CuIn_5S_8$ single-unit-cell layers. (b) Photocatalytic CO_2 reduction performances of $CuIn_5S_8$ (blue bars) and Vs-$CuIn_5S_8$ (red bars) single-unit-cell layers. (c, d) Free energy diagrams of CO_2 photoreduction to CH_4 for the Vs-$CuIn_5S_8$ and pristine $CuIn_5S_8$ single-unit-cell layers (Reproduced from Ref. [55] with permission).

Furthermore, the large specific surface area of CMS nanomaterials could bring a huge number of reactive sites, thus leading to excellent photocatalytic performance. For example, single-phase Cu_3SnS_4 with a bandgap of 1.76 eV is a robust photocatalyst that can selectively reduce CO_2 into CH_4 via a photocatalytic reaction [147]. The Cu_3SnS_4 photocatalyst exhibited a remarkable CH_4 production rate of 14 μmol g^{-1} h^{-1} with 80% selectivity without a cocatalyst or scavenger. To improve the activity and selectivity of the Cu_3SnS_4 photocatalyst, Yu and coauthors constructed S vacancies in Cu_3SnS_4 nanocrystals to introduce Cu(I) and Sn(II), which can effectively suppress the recombination of electrons and holes and improve their selectivity and reactivity [62]. The as-prepared S-vacancy Cu_3SnS_4 nanocrystals exhibited a CH_4 evolution rate of 22.65 μmol g^{-1} h^{-1} with a selectivity of 83.1%, without any cocatalyst or scavenger. Similarly, Xie and coauthors engineered S vacancies in Cu_5InS_8 single-unit-cells to improve the selectivity of photocatalytic CO_2 reduction (Figure 5a–d) [55]. The existence of S vacancies not only reduce the overall activation energy barrier (Figure 5a), but also transform the endoergic protonation process to an exoergic reaction step (Figure 5c–d), which can change the reaction pathway to improve the selectivity of CH_4. The obtained S-vacancy $CuIn_5S_8$ (Vs-$CuIn_5S_8$) single-unit-cell layers exhibited a CH_4 evolution rate of 8.7 μmol g^{-1} h^{-1} with a near 100% selectivity in the photocatalytic CO_2 reduction reaction (Figure 5b). Wang and coauthors constructed Cu_xInS_5-Cu_ySe S-scheme heterostructures to enhance the reactivity of photocatalytic CO_2 reduction [148]. The obtained S-scheme heterostructures showed a near 100% selectivity for photocatalytic CO_2 reduction to methanol, with a rate of 5.250 μmol g^{-1} h^{-1}. In addition, Cu-based ternary and quaternary sulfide

QDs are usually used as photosensitizers for photocatalytic CO_2 reduction assisted by molecular catalysts [46,149,150]. For example, Weiss and coauthors used CIS colloidal QDs as photosensitizers for the photocatalytic reduction of CO_2 to CO in pure water [46]. The photocatalysts exhibited excellent photoreduction performances with a turnover number of 72484−84101, a quantum yield of 0.96%–3.39%, and a CO selectivity of 99%.

3.4. Photocatalytic organic synthesis

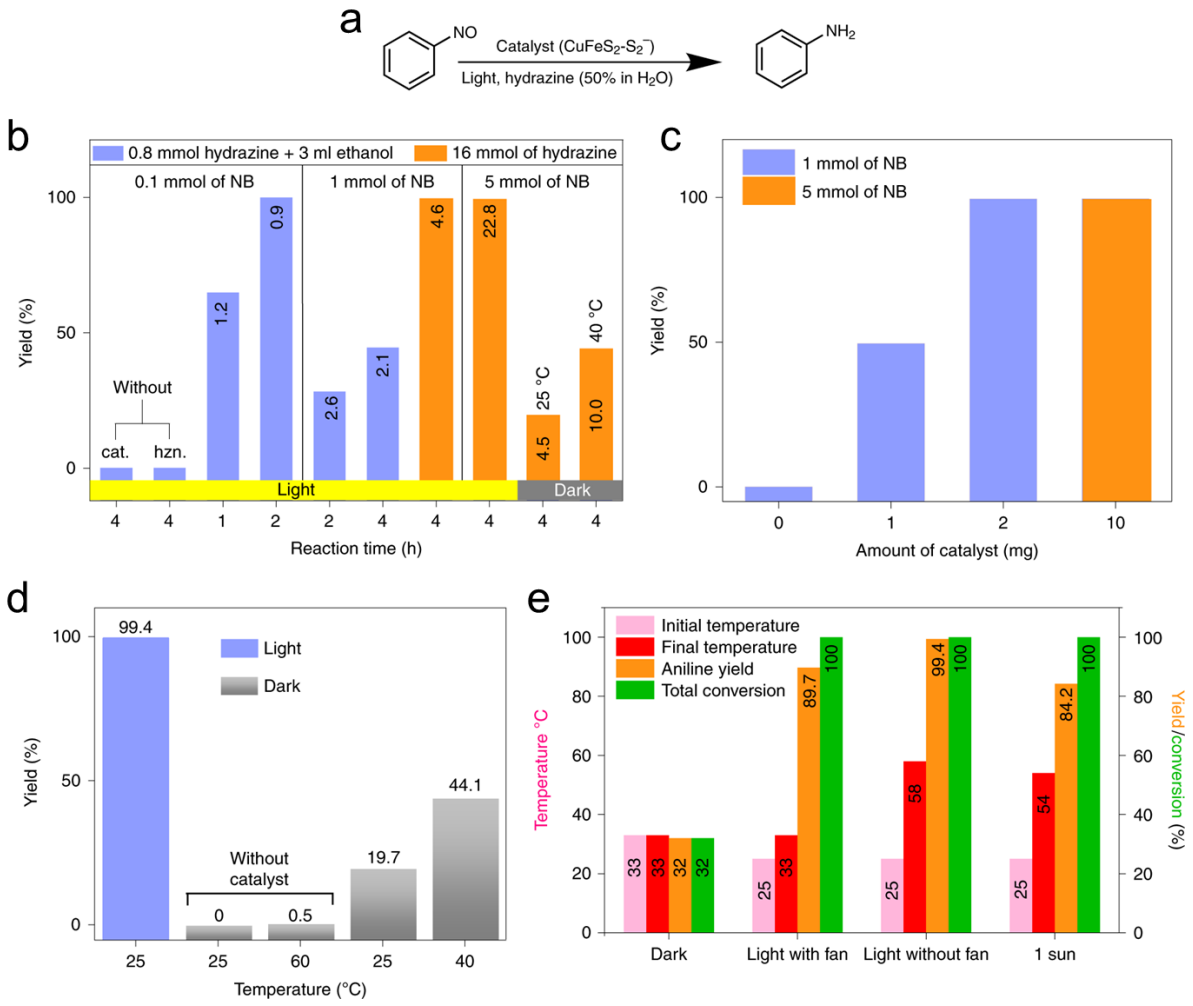

Figure 6. (a) Photocatalytic reduction of nitrobenzene (NB) using CFS nanocrystals. (b) Photocatalytic reduction of NB for different reaction times. (c) Photocatalytic reduction of NB with different amounts of NB and catalysts. (d, e) Photocatalytic aniline yield at controlled temperature or light [151].

Photocatalytic organic synthesis is not only an attractive strategy enabling direct solar energy to chemical energy conversion, but it also provides a promising alternative to traditional high-energy chemical synthesis. Photocatalysts can absorb solar light to produce electrons and holes, thereby promoting chemical reactions on the surface of photocatalysts. A series of classic reactions, such as alcohol oxidation, hydrogenation, aerobic coupling and epoxidation have been achieved via

photocatalytic reactions. Note that, the photocatalyst is essential for the photocatalytic reaction. CMSs are widely used for photocatalytic organic synthesis, such as PEC methylcyclohexane synthesis and PEC ammonia synthesis [47,152].

The development of nanotechnology promotes the preferable use of CMS nanomaterials for photocatalytic organic synthesis. For example, chalcopyrite CFS nanocrystals with a tetragonal structure show obvious localized surface plasmon resonance at 2.4 eV, which relaxes through nonradiative damping, thus generating hot holes or electrons and heat. In addition, due to their strong coordination preference of Fe–S units for organics and hydrogen atoms, CFS nanocrystals could be used as an attractive plasmonic photocatalyst for photocatalytic synthesis [151,153]. Zbořil and coauthors used CFS nanocrystals as plasmonic photocatalysts for the selective hydrogenation of nitroaromatics (Figure 6a–e) [151]. Under solar light irradiation, the CFS nanocrystals work through the synthetic action of photothermal effects and hot holes. The CFS nanocrystal catalysts exhibited a higher production rate than other top-rated photo and thermal catalysts. Importantly, these plasmonic catalysts can be reused many times. Sun and coauthors used S-doped biochar-supported CIS QD-sensitized Bi_2MoO_6 hierarchical flowers as photocatalysts for efficient photocatalytic biorefineries [154]. The obtained photocatalyst exhibited a xylonic acid yield of 86.59% under visible light irradiation. Chen and coauthors constructed a CIS modified polymeric carbon nitride S-scheme photocatalyst for H_2O_2 synthesis [155]. The optimized S-scheme photocatalyst showed a H_2O_2 yield of 1247.6 μmol L^{-1} h^{-1} with an apparent quantum yield (AQY) of 16.0% at 420 nm.

3.5. Photocatalytic pollutant removal

A pollutant-free environment is a fundamental need of human beings. A variety of pollutants effect living organisms. To solve these problems, the exploration of catalysts for the photocatalytic degradation of these pollutants using solar energy is necessary [156,157]. Semiconductor photocatalysis is an economical and effective strategy to remove pollutants. Metal oxide semiconductors are the most commonly used photocatalysts for photocatalytic pollutant removal [158,159]. Meanwhile, the greatest disadvantage of these photocatalysts is their wide bandgap which limits the absorption of visible light. CMS is a promising candidate for metal oxide due to its wide light absorption range [49,160–162].

Under visible light irradiation, CMS photocatalysts absorb light to produce hole-electron pairs. Then, the electrons and holes migrate to the surface of the photocatalysts. Finally, the hole-electron pairs format different reactive oxygen species via a series of redox reactions, which are the dominant active species in the photooxidation of pollutants (Figure 7a). CTS flower-like architectures show obvious photocatalytic activity for photodegradation of methylene blue [163]. CZTS nanoparticles with a size of 2–5 nm was used for the photocatalytic degradation of industrial waste and organic pollutants in water [49]. The efficiency of CZTS nanoparticles was 75% for industrial waste and 98.4% for organic pollutants under sunlight (Figure 7b,c). Deka and coauthors also used surfactant-free hydrophilic CZTS nanoparticles as photocatalysts for the photoreduction of Cr(IV) into nontoxic Cr(III) [164]. The high catalytic performance of the as-prepared CZTS NPs under visible light irradiation is attributed to the size, surface charge and electronic effect of the CZTS nanoparticles.

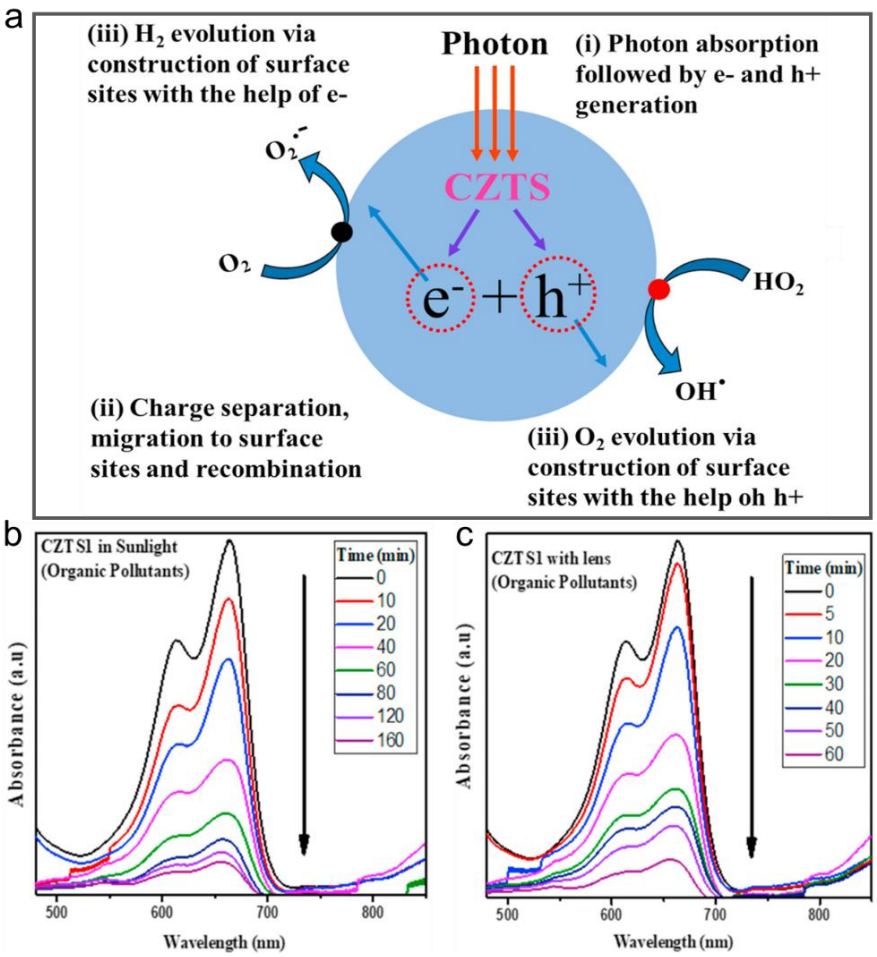

Figure 7. (a) Photocatalytic pollutant removal mechanism of CZTS. (b, c) Absorption spectra for CZTS (organic pollutants) in sunlight and with lens [49].

4. Conclusions

Due to their suitable bandgap, adjustable atomic structure, unique electronic state, and outstanding optoelectronic properties, CMS nanomaterials are widely used in the field of photocatalysis and show exciting photocatalytic performances. This review provides a summary of recent progress on the photocatalytic applications of Cu-based ternary and quaternary sulfide nanomaterials, such as photocatalytic H_2 production, CO_2 reduction, organic synthesis, pollutant removal and PEC H_2 production.

Although remarkable progress has been made in the photocatalytic applications of Cu-based ternary and quaternary sulfide nanomaterials, there is a series of challenges that merit further investigation. First, the photocatalytic performances of current CMS nanomaterials are deficient for feasible scale applications. It is necessary to develop other CMS nanomaterials with novel structural features and electronic properties for photocatalytic applications. Additionally, engineering strategies should be developed to improve the photocatalytic performances of CMS nanomaterials, such as surface and defect engineering, element doping, cocatalyst loading, crystal structure engineering, and homojunction and heterojunction construction. Second, it is necessary to study the detailed photocatalytic mechanisms of how the CMS photocatalysts work using in situ methods, such as X-ray photoelectron spectroscopy (XPS), Fourier transform infrared spectroscopy, X-ray absorption fine

structure (XAFS), Raman spectroscopy, and HRTEM. Deep exploration of the intrinsic mechanism of CMS photocatalysts will be beneficial for rational photocatalyst design to obtain higher photocatalytic activity. Third, the theoretical study of the CMS photocatalysis process is insufficient. Due to the surface atomic reconstruction and dynamic exciton behavior during the photocatalytic reaction, it is significant to use time-dependent density functional theory calculations to explore the excited-state chemistry. Furthermore, in situ characterizations assisted by calculations will provide deep insights into the relationship between atomic arrangements and photocatalytic properties. Fourth, the main products are CH_4 and CO for the photocatalytic CO_2 reduction of CMS nanomaterials. However, it is difficult to obtain high value-added C2+ products. Finally, hole-generated photocorrosion is a general problem for the metal sulfide photocatalysts. Further efforts should be made to develop other means of addressing the stability problems coming from photocorrosion.

Use of AI tools declaration

The author declares that no Artificial Intelligence (AI) tools were used in the creation of this article.

Acknowledgments

This work was supported by the National Key Research and Development Program of China (Grants 2021YFA0715700), the National Natural Science Foundation of China (Grants 22101271).

Conflict of interest

The author declares no conflict of interest.

References

1. Parvulescu VI, Epron F, Garcia H, et al. (2021) Recent progress and prospects in catalytic water treatment. *Chem Rev* 122: 2981–3121. https://doi.org/10.1021/acs.chemrev.1c00527
2. Wang Q, Domen K (2020) Particulate photocatalysts for light-driven water splitting: Mechanisms, challenges, and design strategies. *Chem Rev* 120: 919–985. https://doi.org/10.1021/acs.chemrev.9b00201
3. Rahman MZ, Edvinsson T, Gascon J (2022) Hole utilization in solar hydrogen production. *Nat Rev Chem* 6: 243–258. https://doi.org/10.1038/s41570-022-00366-w
4. Zhou P, Luo M, Guo S (2022) Optimizing the semiconductor-metal-single-atom interaction for photocatalytic reactivity. *Nat Rev Chem* 6: 823–838. https://doi.org/10.1038/s41570-022-00434-1
5. Sokol KP, Andrei V (2022) Automated synthesis and characterization techniques for solar fuel production. *Nat Rev Mater* 7: 251–253. https://doi.org/10.1038/s41578-022-00432-1
6. Chen S, Takata T, Domen K (2017) Particulate photocatalysts for overall water splitting. *Nat Rev Mater* 2: 17050. http://doi.org/10.1038/natrevmats.2017.50
7. Chang K, Hai X, Ye JH (2016) Transition metal disulfides as noble-metal-alternative co-catalysts for solar hydrogen production. *Adv Energy Mater* 6: 1502555. https://doi.org/10.1002/aenm.201502555

8. Wang F, Li Q, Xu D (2017) Recent progress in semiconductor-based nanocomposite photocatalysts for solar-to-chemical energy conversion. *Adv Energy Mater* 7: 1700529. https://doi.org/10.1002/aenm.201700529
9. Fu CF, Wu X, Yang J (2018) Material design for photocatalytic water splitting from a theoretical perspective. *Adv Mater* 30: e1802106. https://doi.org/10.1002/adma.201802106
10. Li H, Zhou Y, Tu W, et al. (2015) State-of-the-art progress in diverse heterostructured photocatalysts toward promoting photocatalytic performance. *Adv Funct Mater* 25: 998–1013. http://doi.org/10.1002/adfm.201401636
11. Sun X, Zhang X, Xie Y (2020) Surface defects in two-dimensional photocatalysts for efficient organic synthesis. *Matter* 2: 842–861. https://doi.org/10.1016/j.matt.2020.02.006
12. Fan W, Zhang Q, Wang Y (2014) Semiconductor-based nanocomposites for photocatalytic H_2 production and CO_2 conversion. *Phys Chem Chem Phys* 15: 2632–2649. http://doi.org/10.1039/C2CP43524A
13. Zhang N, Gao C, Xiong Y (2019) Defect engineering: A versatile tool for tuning the activation of key molecules in photocatalytic reactions. *J Energy Chem* 37: 43–57. https://doi.org/10.1016/j.jechem.2018.09.010
14. Talapin DV, Lee JS, Kovalenko MV, et al. (2010) Prospects of colloidal nanocrystals for electronic and optoelectronic applications. *Chem Rev* 110: 389–458. https://doi.org/10.1021/cr900137k
15. Savage KJ, Hawkeye MM, Esteban R, et al. (2012) Revealing the quantum regime in tunnelling plasmonics. *Nature* 491: 574–577. https://doi.org/10.1038/nature11653
16. Meinardi F, Ehrenberg S, Dhamo L, et al. (2017) Highly efficient luminescent solar concentrators based on earth-abundant indirect-bandgap silicon quantum dots. *Nature Photon* 11: 177–185. https://doi.org/10.1038/nphoton.2017.5
17. Smith AM, Mohs AM, Nie S (2019) Tuning the optical and electronic properties of colloidal nanocrystals by lattice strain. *Nature Nanotech* 4: 56–63. https://doi.org/10.1038/nnano.2008.360
18. Oh N, Kim BH, Cho SY, et al. (2017) Double-heterojunction nanorod light-responsive LEDs for display applications. *Science* 355: 616–619. https://doi.org/10.1126/science.aal2038
19. Du J, Singh R, Fedin I, et al. (2020) Spectroscopic insights into high defect tolerance of Zn: $CuInSe_2$ quantum-dot-sensitized solar cells. *Nat Energy* 5: 409–417. https://doi.org/10.1038/s41560-020-0617-6
20. Chen R, Ren Z, Liang Y, et al. (2022) Spatiotemporal imaging of charge transfer in photocatalyst particles. *Nature* 610: 296–301. https://doi.org/10.1038/s41586-022-05183-1
21. Zhou P, Navid IA, Ma Y, et al. (2023) Solar-to-hydrogen efficiency of more than 9% in photocatalytic water splitting. *Nature* 613: 66–70. https://doi.org/10.1038/s41586-022-05399-1
22. Chen X, Liu L, Yu PY, et al. (2011) Increasing solar absorption for photocatalysis with black hydrogenated titanium dioxide nanocrystals. *Science* 331: 746–750. https://doi.org/10.1126/science.1200448
23. Lotfi S, Fischer K, Schulze A, et al. (2022) Photocatalytic degradation of steroid hormone micropollutants by TiO_2-coated polyethersulfone membranes in a continuous flow-through process. *Nature Nanotech* 17: 417–423. https://doi.org/10.1038/s41565-022-01074-8
24. Song S, Song H, Li L, et al. (2021) A selective Au-ZnO/TiO_2 hybrid photocatalyst for oxidative coupling of methane to ethane with dioxygen. *Nat Catal* 4: 1032–1042. https://doi.org/10.1038/s41929-021-00708-9

25. Lin R, Wan J, Xiong Y, et al. (2018) Quantitative study of charge carrier dynamics in well-defined WO_3 nanowires and nanosheets: Insight into the crystal facet effect in photocatalysis. *J Am Chem Soc* 140: 9078–9082. https://doi.org/10.1021/jacs.8b05293
26. Simon T, Bouchonville N, Berr MJ, et al. (2014) Redox shuttle mechanism enhances photocatalytic H_2 generation on Ni-decorated CdS nanorods. *Nat Mater* 13: 1013–1018. https://doi.org/10.1038/nmat4049
27. Han Z, Qiu F, Eisenberg R, et al. (2012) Robust photogeneration of H_2 in water using semiconductor nanocrystals and a nickel catalyst. *Science* 338: 1321–1324. https://doi.org/10.1126/science.1227775
28. Lin L, Lin Z, Zhang J, et al. (2020) Molecular-level insights on the reactive facet of carbon nitride single crystals photocatalysing overall water splitting. *Nat Catal* 3: 649–655. https://doi.org/10.1038/s41929-020-0476-3
29. Takata T, Jiang J, Sakata Y, et al. (2020) Photocatalytic water splitting with a quantum efficiency of almost unity. *Nature* 581: 411–414. https://doi.org/10.1038/s41586-020-2278-9
30. Regulacio MD, Han MY (2016) Multinary I-III-VI_2 and I_2-II-IV-VI_4 semiconductor nanostructures for photocatalytic applications. *Acc Chem Res* 49: 511–519. https://doi.org/10.1021/acs.accounts.5b00535
31. Ha E, Lee LY, Wang J, et al. (2014) Significant enhancement in photocatalytic reduction of water to hydrogen by Au/Cu_2ZnSnS_4 nanostructure. *Adv Mater* 26: 3496–3500. https://doi.org/10.1002/adma.201400243
32. Ye C, Regulacio MD, Lim SH, et al. (2012) Alloyed $(ZnS)_x(CuInS_2)_{(1-x)}$ semiconductor nanorods: Synthesis, bandgap tuning and photocatalytic properties. *Chem Eur J* 18: 11258–11263. https://doi.org/10.1002/chem.201201626
33. Li H, Li WJ, Li W, et al. (2020) Engineering crystal phase of polytypic $CuInS_2$ nanosheets for enhanced photocatalytic and photoelectrochemical performance. *Nano Res* 13: 583–590. https://doi.org/10.1007/s12274-020-2665-4
34. Kageshima Y, Shiga S, Ode T, et al. (2021) Photocatalytic and photoelectrochemical hydrogen evolution from water over $Cu_2SnxGe_{1-x}S_3$ particles. *J Am Chem Soc* 143: 5698–5708. https://doi.org/10.1021/jacs.0c12140
35. Fan FJ, Wu L, Yu SH (2013) Energetic I–III–VI_2 and I_2–II–IV–VI_4 nanocrystals: Synthesis, photovoltaic and thermoelectric applications. *Energy Environ Sci* 7: 190–208. https://doi.org/10.1039/C3EE41437J
36. Chang ZX, Zhou WH, Kou DX, et al. (2014) Phase-dependent photocatalytic H_2 evolution of copper zinc tin sulfide under visible light. *Chem Commun* 50: 12726–12729. https://doi.org/10.1039/c4cc05654j
37. Liu Q, Zhao Z, Lin Y, et al. (2011) Alloyed $(ZnS)_x(Cu_2SnS_3)_{1-x}$ and $(CuInS_2)_x(Cu_2SnS_3)_{1-x}$ nanocrystals with arbitrary composition and broad tunable band gaps. *Chem Commun* 47: 964–966. http://doi.org/10.1039/C0CC03560B
38. Tan L, Liu Y, Mao B, et al. (2018) Effective bandgap narrowing of Cu-In-Zn-S quantum dots for photocatalytic H_2 production via cocatalyst-alleviated charge recombination. *Inorg Chem Front* 5: 258–265. http://doi.org/10.1039/C7QI00607A
39. Wu L, Su F, Liu T, et al. (2022) Phosphorus-doped single-crystalline quaternary sulfide nanobelts enable efficient visible-light photocatalytic hydrogen evolution. *J Am Chem Soc* 144: 20620–20629. https://doi.org/10.1021/jacs.2c07313

40. Wu L, Wang Q, Zhuang TT, et al. (2020) Single crystalline quaternary sulfide nanobelts for efficient solar-to-hydrogen conversion. *Nat Commun* 11: 5194. https://doi.org/10.1038/s41467-020-18679-z
41. Li Y, Wang Y, Pattengale B, et al. (2017) High-index faceted $CuFeS_2$ nanosheets with enhanced behavior for boosting hydrogen evolution reaction. *Nanoscale* 9: 9230–9237. https://doi.org/10.1039/C7NR03182C
42. Zhang X, Xu Y, Zhang J, et al. (2018) Synthesis of wurtzite Cu_2ZnSnS_4 nanosheets with exposed high-energy (002) facets for fabrication of efficient Pt-free solar cell counter electrodes. *Sci Rep* 8: 248. https://doi.org/10.1038/s41598-017-18631-0
43. Wu L, Wang Q, Zhuang TT, et al. (2022) A library of polytypic copper-based quaternary sulfide nanocrystals enables efficient solar-to-hydrogen conversion. *Nat Commun* 13: 5414. https://doi.org/10.1038/s41467-022-33065-7
44. Chen SY, Gong XG, Walsh A, et al. (2009) Electronic structure and stability of quaternary chalcogenide semiconductors derived from cation cross-substitution of II-VI and I-III-VI_2 compounds. *Phys Rev B* 79: 165211. https://doi.org/10.1103/PhysRevB.79.165211
45. Ozel F, Aslan E, Istanbullu B, et al. (2016) Photocatalytic hydrogen evolution based on Cu_2ZnSnS_4, Cu_2NiSnS_4 and Cu_2CoSnS_4 nanocrystals. *Appl Catal B-Environ* 198: 67–73. https://doi.org/10.1016/j.apcatb.2016.05.053
46. Arcudi F, Đorđević L, Nagasing B, et al. (2021) Quantum dot-sensitized photoreduction of CO_2 in water with turnover number >80,000. *J Am Chem Soc* 143: 18131–18138. https://doi.org/10.1021/jacs.1c06961
47. Wang P, Minegishi T, Ma G, et al. (2012) Photoelectrochemical conversion of toluene to methylcyclohexane as an organic hydride by Cu_2ZnSnS_4-based photoelectrode assemblies. *J Am Chem Soc* 134: 2469–2472. https://doi.org/10.1021/ja209869k
48. Huang DW, Wang K, Yu L, et al. (2018) Over 1% efficient unbiased stable solar water splitting based on a sprayed Cu_2ZnSnS_4 photocathode protected by a HfO_2 photocorrosion-resistant film. *Acs Energy Lett* 3: 1875–1881. https://doi.org/10.1021/acsenergylett.8b01005
49. Semalti P, Sharma V, Sharma SN (2021) A novel method of water remediation of organic pollutants and industrial wastes by solution-route processed CZTS nanocrystals. *J Materiomics* 7: 904–919. https://doi.org/10.1016/j.jmat.2021.04.005
50. Akkerman QA, Genovese A, George C, et al. (2015) From binary Cu_2S to ternary Cu-In-S and quaternary Cu-In-Zn-S nanocrystals with tunable composition via partial cation exchange. *ACS Nano* 9: 521–531. https://doi.org/10.1021/nn505786d
51. De Trizio L, Li H, Casu A, et al. (2014) Sn cation valency dependence in cation exchange reactions involving $Cu_{2-x}Se$ nanocrystals. *J Am Chem Soc* 136: 16277–16284. https://doi.org/10.1021/ja508161c
52. Pan D, An L, Sun Z, et al. (2018) Synthesis of Cu−In−S ternary nanocrystals with tunable structure and composition. *J Am Chem Soc* 130: 5620–5621. https://doi.org/10.1021/ja711027j
53. Akkari FC, Abdelkader D, Gallas B, et al. (2017) Ellipsometric characterization and optical anisotropy of nanostructured $CuIn_3S_5$ and $CuIn_5S_8$ thin films. *Mat Sci Semicon Proc* 71: 156–160. https://doi.org/10.1016/j.mssp.2017.07.023
54. Khemiri N, Kanzari M (2010) Comparative study of structural and morphological properties of $CuIn_3S_5$ and $CuIn_7S_{11}$ materials. *Nucl Instrum Meth B* 268: 268–272. https://doi.org/10.1016/j.nimb.2009.10.175

55. Li XD, Sun YF, Xu JQ, et al. (2019) Selective visible-light-driven photocatalytic CO_2 reduction to CH_4 mediated by atomically thin $CuIn_5S_8$ layers. *Nat Energy* 4: 690–699. https://doi.org/10.1038/s41560-019-0431-1
56. Ng C, Yun JH, Tan HL, et al. (2018) A dual-electrolyte system for photoelectrochemical hydrogen generation using $CuInS_2$-In_2O_3-TiO_2 nanotube array thin film. *Sci China Mater* 61: 895–904. https://doi.org/10.1007/s40843-017-9237-2
57. Xu W, Xie ZZ, Han WJ, et al. (2022) Rational design of interfacial energy level matching for $CuGaS_2$ based photocatalysts over hydrogen evolution reaction. *Int J Hydrogen Energy* 47: 11853–11862. https://doi.org/ 10.1016/j.ijhydene.2022.01.209
58. Ghorpade UV, Suryawanshi MP, Shin SW, et al. (2016) Colloidal wurtzite Cu_2SnS_3 (CTS) nanocrystals and their applications in solar cells. *Chem Mater* 28: 3308–3317. https://doi.org/10.1021/acs.chemmater.6b00176
59. Jathar SB, Rondiya SR, Jadhav YA, et al. (2021) Ternary Cu_2SnS_3: Synthesis, structure, photoelectrochemical activity, and heterojunction band offset and alignment. *Chem Mater* 33: 1983–1993. https://doi.org/10.1021/acs.chemmater.0c03223
60. Yi LX, Wang D, Gao MY (2012) Synthesis of Cu_3SnS_4 nanocrystals and nanosheets by using $Cu_{31}S_{16}$ as seeds. *CrystEngComm* 14: 401–404. https://doi.org/10.1039/C1ce06153d
61. Lin J, Lim JM, Youn DH, et al. (2019) Cu_4SnS_4-rich nanomaterials for thin-film lithium batteries with enhanced conversion reaction. *ACS Nano* 13: 10671–10681. https://doi.org/10.1021/acsnano.9b05029
62. Wang J, Bo T, Shao B, et al. (2021) Effect of S vacancy in Cu_3SnS_4 on high selectivity and activity of photocatalytic CO_2 reduction. *Appl Catal B-Environ* 297: 120498. https://doi.org/10.1016/j.apcatb.2021.120498
63. Kamemoto S, Matsuda Y, Takahashi M, et al. (2022) Photocatalytic water splitting on Cu_2SnS_3 photoelectrode: Effects of Cu/Sn composite ratio on the photoelectrochemical performance. *Catal Today* 411–412: 113820. https://doi.org/10.1016/j.cattod.2022.06.035
64. An X, Kays JC, Lightcap IV, et al. (2022) Wavelength-dependent bifunctional plasmonic photocatalysis in Au/chalcopyrite hybrid nanostructures. *ACS Nano* 16: 6813–6824. https://doi.org/10.1021/acsnano.2c01706
65. Sugathan A, Bhattacharyya B, Kishore VVR, et al. (2018) Why does $CuFeS_2$ resemble gold? *J Phys Chem Lett* 9: 696–701. https://doi.org/10.1021/acs.jpclett.7b03190
66. Bhattacharyya B, Pandey A (2016) $CuFeS_2$ quantum dots and highly luminescent $CuFeS_2$ based core/shell structures: Synthesis, tunability, and photophysics. *J Am Chem Soc* 138: 10207–10213. https://doi.org/10.1021/jacs.6b04981
67. Tsuji I, Kato H, Kobayashi H, et al. (2005) Photocatalytic H_2 evolution under visible-light irradiation over band-structure-controlled $(CuIn)_xZn_{2(1-x)}S_2$ solid solutions. *J Phys Chem B* 109: 7323–7329. https://doi.org/10.1021/jp044722e
68. Goodman CHL (1958) The prediction of semiconducting properties in inorganic compounds. *J Phys Chem Solids* 6: 305–314. https://doi.org/10.1016/0022-3697(58)90050-7
69. Yan C, Huang J, Sun K, et al. (2018) Cu_2ZnSnS_4 solar cells with over 10% power conversion efficiency enabled by heterojunction heat treatment. *Nat Energy* 3: 764–772. https://doi.org/10.1038/s41560-018-0206-0

70. De Trizio L, Prato M, Genovese A, et al. (2012) Strongly fluorescent quaternary Cu–In–Zn–S nanocrystals prepared from $Cu_{1-x}InS_2$ nanocrystals by partial cation exchange. *Chem Mater* 24: 2400–2406. https://doi.org/10.1021/cm301211e
71. Cui Y, Wang G, Pan D (2012) Synthesis and photoresponse of novel Cu_2CdSnS_4 semiconductor nanorods. *J Mater Chem* 22: 12471. https://doi.org/10.1039/c2jm32034g
72. Ikeda S, Fujikawa S, Harada T, et al. (2019) Photocathode characteristics of a spray-deposited Cu_2ZnGeS_4 thin film for CO_2 reduction in a CO_2-saturated aqueous solution. *ACS Appl Energy Mater* 2: 6911–6918. https://doi.org/10.1021/acsaem.9b01418
73. Singh A, Singh A, Ciston J, et al. (2015) Synergistic role of dopants on the morphology of alloyed copper chalcogenide nanocrystals. *J Am Chem Soc* 137: 6464–6467. https://doi.org/10.1021/jacs.5b02880
74. Huang S, He Q, Zai J, et al. (2015) The role of Mott–Schottky heterojunctions in PtCo–Cu_2ZnGeS_4 as counter electrodes in dye-sensitized solar cells. *Chem Commun* 51: 8950–8953. http://doi.org/10.1039/C5CC02584B
75. Septina W, Gunawan, Ikeda S, et al. (2015) Photosplitting of water from wide-gap $Cu(In,Ga)S_2$ thin films modified with a CdS layer and Pt nanoparticles for a high-onset-potential photocathode. *J Phys Chem C* 119: 8576–8583. http://doi.org/10.1021/acs.jpcc.5b02068
76. Liu XY, Zhang G, Chen H, et al. (2017) Efficient defect-controlled photocatalytic hydrogen generation based on near-infrared Cu-In-Zn-S quantum dots. *Nano Res* 11: 1379–1388. https://doi.org/10.1007/s12274-017-1752-7
77. Ye C, Regulacio MD, Lim SH, et al. (2015) Alloyed ZnS-$CuInS_2$ semiconductor nanorods and their nanoscale heterostructures for visible-light-driven photocatalytic hydrogen generation. *Chem Eur J* 21: 9514–9519. https://doi.org/10.1002/chem.201500781
78. Chen FK, Zai JT, Xu M, et al. (2013) 3D-hierarchical Cu_3SnS_4 flowerlike microspheres: Controlled synthesis, formation mechanism and photocatalytic activity for H_2 evolution from water. *J Mater Chem A* 1: 4316–4323. https://doi.org/10.1039/C3ta01491f
79. Zhang P, Wang T, Chang X, et al. (2016) Effective charge carrier utilization in photocatalytic conversions. *Acc Chem Res* 49: 911–921. http://doi.org/10.1021/acs.accounts.6b00036
80. Wei Y, Yang N, Huang K, et al. (2020) Steering hollow multishelled structures in photocatalysis: Optimizing surface and mass transport. *Adv Mater* 32: e2002556. http://doi.org/10.1002/adma.202002556
81. Chen Q, Liu Y, Gu X, et al. (2022) Carbon dots mediated charge sinking effect for boosting hydrogen evolution in Cu-In-Zn-S QDs/MoS_2 photocatalysts. *Appl Catal B-Environ* 301: 120755. http://doi.org/10.1016/j.apcatb.2021.120755
82. Yu X, Shavel A, An X, et al. (2014) Cu_2ZnSnS_4-Pt and Cu_2ZnSnS_4-Au heterostructured nanoparticles for photocatalytic water splitting and pollutant degradation. *J Am Chem Soc* 136: 9236–9239. http://doi.org/10.1021/ja502076b
83. Ali N, Tsega TT, Cao Y, et al. (2021) Copper vacancy activated plasmonic $Cu_{3-x}SnS_4$ for highly efficient photocatalytic hydrogen generation: Broad solar absorption, efficient charge separation and decreased HER overpotential. *Nano Res* 14: 3358–3364. https://doi.org/10.1007/s12274-021-3604-8
84. Fan XB, Yu S, Zhan F, et al. (2017) Nonstoichiometric Cu_xIn_yS quantum dots for efficient photocatalytic hydrogen evolution. *ChemSusChem* 10: 4833–4838. https://doi.org/10.1002/cssc.201701950

85. Yu X, An X, Genç A, et al. (2015) Cu_2ZnSnS_4–PtM (M = Co, Ni) nanoheterostructures for photocatalytic hydrogen evolution. *J Phys Chem C* 119: 21882–21888. http://doi.org/10.1021/acs.jpcc.5b06199
86. Lin T, Yang T, Cai Y, et al. (2023) Transformation-optics-designed plasmonic singularities for efficient photocatalytic hydrogen evolution at metal/semiconductor interfaces. *Nano Lett* 23: 5288–5296. http://doi.org/10.1021/acs.nanolett.3c01287
87. Jiang F, Pan B, You D, et al. (2016) Visible light photocatalytic H_2-production activity of epitaxial Cu_2ZnSnS_4/ZnS heterojunction. *Catal Commun* 85: 39–43. http://doi.org/10.1016/j.catcom.2016.07.017
88. Yuan M, Wang JL, Zhou WH, et al. (2017) Cu_2ZnSnS_4-CdS heterostructured nanocrystals for enhanced photocatalytic hydrogen production. *Catal Sci Technol* 7: 3980–3984. http://doi.org/10.1039/c7cy01360d
89. Yuan M, Zhou WH, Kou DX, et al. (2018) Cu_2ZnSnS_4 decorated CdS nanorods for enhanced visible-light-driven photocatalytic hydrogen production. *Int J Hydrogen Energy* 43: 20408–20416. https://doi.org/10.1016/j.ijhydene.2018.09.161
90. Zhuang TT, Yu P, Fan FJ, et al. (2014) Controlled synthesis of kinked ultrathin ZnS nanorods/nanowires triggered by chloride ions: A case study. *Small* 10: 1394–1402. https://doi.org/10.1002/smll.201302656
91. Li Y, Zhuang TT, Fan F, et al. (2018) Pulsed axial epitaxy of colloidal quantum dots in nanowires enables facet-selective passivation. *Nat Commun* 9: 4947. https://doi.org/10.1038/s41467-018-07422-4
92. Li M, Zhao Z, Cheng T, et al. (2016) Ultrafine jagged platinum nanowires enable ultrahigh mass activity for the oxygen reduction reaction. *Science* 354: 1414–1419. https://doi.org/10.1126/science.aaf9050
93. Chen D, Zhang H, Li Y, et al. (2018) Spontaneous formation of noble- and heavy-metal-free alloyed semiconductor quantum rods for efficient photocatalysis. *Adv Mater* 30: e1803351. https://doi.org/10.1002/adma.201803351
94. Zhang Z, Wu Q, Johnson G, et al. (2019) Generalized synthetic strategy for transition-metal-doped brookite-phase TiO_2 nanorods. *J Am Chem Soc* 141: 16548–16552. https://doi.org/10.1021/jacs.9b06389
95. Gonce MK, Aslan E, Ozel F, et al. (2016) Dye-sensitized Cu_2XSnS_4 (X = Zn, Ni, Fe, Co, and Mn) nanofibers for efficient photocatalytic hydrogen evolution. *ChemSusChem* 9: 600–605. http://doi.org/10.1002/cssc.201501661
96. Zhou Y, Zhang Y, Lin M, et al. (2015) Monolayered Bi_2WO_6 nanosheets mimicking heterojunction interface with open surfaces for photocatalysis. *Nat Commun* 6: 8340. http://doi.org/10.1038/ncomms9340
97. Tian B, Tian B, Smith B, et al. (2018) Facile bottom-up synthesis of partially oxidized black phosphorus nanosheets as metal-free photocatalyst for hydrogen evolution. *Proc Natl Acad Sci* 115: 4345–4350. http://doi.org/10.1073/pnas.1800069115
98. Nishioka S, Hojo K, Xiao L, et al. (2022) Surface-modified, dye-sensitized niobate nanosheets enabling an efficient solar-driven Z-scheme for overall water splitting. *Sci Adv* 8: eadc9115. https://doi.org/10.1126/sciadv.adc9115
99. Ganguly P, Harb M, Cao Z, et al. (2019) 2D Nanomaterials for photocatalytic hydrogen production. *ACS Energy Lett* 4: 1687–1709. https://doi.org/10.1021/acsenergylett.9b00940

100. Wang L, Wang W, Sun S (2012) A simple template-free synthesis of ultrathin Cu_2ZnSnS_4 nanosheets for highly stable photocatalytic H_2 evolution. *J Mater Chem* 22: 6553–6555. https://doi.org/10.1039/c2jm16515e
101. Zheng L, Xu Y, Song Y, et al. (2009) Nearly monodisperse $CuInS_2$ hierarchical microarchitectures for photocatalytic H_2 evolution under visible light. *Inorg Chem* 48: 4003–4009. https://doi.org/10.1021/ic802399f
102. Huang Y, Chen J, Zou W, et al. (2015) Enhanced photocatalytic hydrogen evolution efficiency using hollow microspheres of $(CuIn)_xZn_{2(1-x)}S_2$ solid solutions. *Dalton Trans* 44: 10991–10996. https://doi.org/10.1039/c5dt01269d
103. Chen Y, Qin Z, Guo X, et al. (2016) One-step hydrothermal synthesis of $(CuIn)_{0.2}Zn_{1.6}S_2$ hollow sub-microspheres for efficient visible-light-driven photocatalytic hydrogen generation. *Int J Hydrogen Energy* 41: 1524–1534. https://doi.org/10.1016/j.ijhydene.2015.11.087
104. Li M, Zhao RJ, Su YJ, et al. (2016) Hierarchically $CuInS_2$ nanosheet-constructed nanowire arrays for photoelectrochemical water splitting. *Adv Mater Interfaces* 3: 1600494. https://doi.org/10.1002/admi.201600494
105. Xu J, Hu Z, Zhang J, et al. (2017) Cu_2ZnSnS_4 and $Cu_2ZnSn(S_{1-x}Se_x)_4$ nanocrystals: Room-temperature synthesis and efficient photoelectrochemical water splitting. *J Mater Chem A* 5: 25230–25236. http://doi.org/10.1039/C7TA06628G
106. Han Z, Eisenberg R (2014) Fuel from water: The photochemical generation of hydrogen from water. *Acc Chem Res* 47: 2537–2544. http://doi.org/10.1021/ar5001605
107. Teitsworth TS, Hill DJ, Litvin SR, et al. (2023) Water splitting with silicon p–i–n superlattices suspended in solution. *Nature* 614: 270–274. https://doi.org/10.1038/s41586-022-05549-5
108. Li Z, Li R, Jing H, et al. (2023) Blocking the reverse reactions of overall water splitting on a Rh/GaN–ZnO photocatalyst modified with Al_2O_3. *Nat Catal* 6: 80–88. https://doi.org/10.1038/s41929-022-00907-y
109. Zhang JH, Zhang M, Dong YY, et al. (2022) CdTe/CdSe-sensitized photocathode coupling with Ni-substituted polyoxometalate catalyst for photoelectrochemical generation of hydrogen. *Nano Res* 15: 1347–1354. https://doi.org/10.1007/s12274-021-3663-x
110. Lee S, Ji L, De Palma AC, et al. (2021) Scalable, highly stable Si-based metal-insulator-semiconductor photoanodes for water oxidation fabricated using thin-film reactions and electrodeposition. *Nat Commun* 12: 3982. https://doi.org/10.1038/s41467-021-24229-y
111. Cheng F, Lin G, Hu X, et al. (2019) Porous single-crystalline titanium dioxide at 2 cm scale delivering enhanced photoelectrochemical performance. *Nat Commun* 10: 3618. https://doi.org/10.1038/s41467-019-11623-w
112. Liu Z, Lu X, Chen D (2018) Photoelectrochemical water splitting of $CuInS_2$ photocathode collaborative modified with separated catalysts based on efficient photogenerated electron–hole separation. *ACS Sustainable Chem Eng* 6: 10289–10294. https://doi.org/10.1021/acssuschemeng.8b01607
113. Kaneko H, Minegishi T, Nakabayashi M, et al. (2016) Enhanced hydrogen evolution under simulated sunlight from neutral electrolytes on $(ZnSe)_{0.85}(CuIn_{0.7}Ga_{0.3}Se_2)_{0.15}$ photocathodes prepared by a bilayer method. *Angew Chem Int Ed* 55: 15329–15333. https://doi.org/10.1002/anie.201609202

114. Tay YF, Kaneko H, Chiam SY, et al. (2018) Solution-processed Cd-substituted CZTS photocathode for efficient solar hydrogen evolution from neutral water. *Joule* 2: 537–548. http://doi.org/10.1016/j.joule.2018.01.012
115. Guo P, Xiao Y, Mo R, et al. (2023) Coherent-twinning-enhanced solar water splitting in thin-film Cu_2ZnSnS_4 photocathodes. *ACS Energy Lett* 8: 494–501. https://doi.org/10.1021/acsenergylett.2c02626
116. Yan C, Sun K, Huang J, et al. (2017) Beyond 11% efficient sulfide kesterite $Cu_2Zn_xCd_{1-x}SnS_4$ solar cell: Effects of cadmium alloying. *ACS Energy Lett* 2: 930–936. http://doi.org/10.1021/acsenergylett.7b00129
117. Yang W, Oh Y, Kim J, et al. (2016) Molecular chemistry-controlled hybrid ink-derived efficient Cu_2ZnSnS_4 photocathodes for photoelectrochemical water splitting. *ACS Energy Lett* 1: 1127–1136. https://doi.org/10.1021/acsenergylett.6b00453
118. Mali MG, Yoon H, Joshi BN, et al. (2015) Enhanced photoelectrochemical solar water splitting using a platinum-decorated CIGS/CdS/ZnO photocathode. *ACS Appl Mater Interfaces* 7: 21619–21625. https://doi.org/10.1021/acsami.5b07267
119. Sun W, Ye Y, You Y, et al. (2018) A top-down synthesis of wurtzite Cu_2SnS_3 nanocrystals for efficient photoelectrochemical performance. *J Mater Chem A* 6: 8221–8226. http://doi.org/10.1039/C8TA00851E
120. Li M, Zhao R, Su Y, et al. (2017) Synthesis of $CuInS_2$ nanowire arrays via solution transformation of Cu_2S self-template for enhanced photoelectrochemical performance. *Appl Catal B-Environ* 203: 715–724. https://doi.org/10.1016/j.apcatb.2016.10.051
121. Nishi H, Kuwabata S, Torimoto T (2013) Composition-dependent photoelectrochemical properties of nonstoichiometric Cu_2ZnSnS_4 nanoparticles. *J Phys Chem C* 117: 21055–21063. https://doi.org/10.1021/jp405008m
122. Chen Y, Chuang CH, Lin KC, et al. (2014) Synthesis and photoelectrochemical properties of $(Cu_2Sn)_xZn_{3(1-x)}S_3$ nanocrystal films. *J Phys Chem C* 118: 11954–11963. http://doi.org/10.1021/jp500270d
123. Yokoyama D, Minegishi T, Jimbo K, et al. (2010) H_2 evolution from water on modified Cu_2ZnSnS_4 photoelectrode under solar light. *Appl Phy Express* 3: 101202. https://doi.org/10.1143/APEX.3.101202
124. Wu XJ, Huang X, Qi X, et al. (2014) Copper-based ternary and quaternary semiconductor nanoplates: Templated synthesis, characterization, and photoelectrochemical properties. *Angew Chem Int Ed* 53: 8929–8933. https://doi.org/10.1002/anie.201403655
125. Yang W, Oh Y, Kim J, et al. Photoelectrochemical properties of vertically aligned $CuInS_2$ nanorod arrays prepared via template-assisted growth and transfer. *ACS Appl Mater Interfaces* 8: 425–431. https://doi.org/10.1021/acsami.5b09241
126. Guijarro N, Prevot MS, Sivula K (2014) Enhancing the charge separation in nanocrystalline Cu_2ZnSnS_4 photocathodes for photoelectrochemical application: The role of surface modifications. *J Phys Chem Lett* 5: 3902–3908. https://doi.org/10.1021/jz501996s
127. Patra BK, Khilari S, Pradhan D, et al. (2016) Hybrid dot–disk Au-$CuInS_2$ nanostructures as active photocathode for efficient evolution of hydrogen from water. *Chem Mater* 28: 4358–4366. http://doi.org/10.1021/acs.chemmater.6b01357

128. Hu Y, Pan Y, Wang Z, et al. Lattice distortion induced internal electric field in TiO_2 photoelectrode for efficient charge separation and transfer. *Nat Commun* 11: 2129. https://doi.org/10.1038/s41467-020-15993-4
129. Kang Z, Si H, Zhang S, et al. (2019) Interface engineering for modulation of charge carrier behavior in ZnO photoelectrochemical water splitting. *Adv Funct Mater* 29: 1808032. https://doi.org/10.1002/adfm.201808032
130. You YM, Tong X, Channa AI, et al. (2022) Tailoring the optoelectronic properties of eco-friendly $CuGaS_2$/ZnSe core/shell quantum dots for boosted photoelectrochemical solar hydrogen production. *Ecomat* 4: e12206. https://doi.org/10.1002/eom2.12206
131. Channa AI, Tong X, Xu JY, et al. (2019) Tailored near-infrared-emitting colloidal heterostructured quantum dots with enhanced visible light absorption for high performance photoelectrochemical cells. *J Mater Chem A* 7: 10225–10230. http://doi.org/10.1039/C9TA01052A
132. Wang R, Xu X, Zhang Y, et al. (2015) Functionalized ZnO@TiO_2 nanorod array film loaded with $ZnIn_{0.25}Cu_{0.02}S_{1.395}$ solid-solution: Synthesis, characterization and enhanced visible light driven water splitting. *Nanoscale* 7: 11082–11092. http://doi.org/10.1039/C5NR02127H
133. Wu HL, Li XB, Tung CH, et al. (2018) Recent advances in sensitized photocathodes: From molecular dyes to semiconducting quantum dots. *Adv Sci* 5: 1700684. http://doi.org/10.1002/advs.201700684
134. Li TL, Teng H (2010) Solution synthesis of high-quality $CuInS_2$ quantum dots as sensitizers for TiO_2 photoelectrodes. *J Mater Chem* 20: 3656–3664. https://doi.org/10.1039/b927279h
135. Liu C, Tong X, Channa AI, et al. (2021) Tuning the composition of heavy metal-free quaternary quantum dots for improved photoelectrochemical performance. *J Mater Chem A* 9: 5825–5832. http://doi.org/10.1039/D0TA11481B
136. Liu Q, Cao F, Wu F, et al. (2016) Partial ion exchange derived 2D Cu–Zn–In–S nanosheets as sensitizers of 1D TiO_2 nanorods for boosting solar water splitting. *ACS Appl Mater Interfaces* 8: 26235–26243. http://doi.org/10.1021/acsami.6b08648
137. Jiang Z, Xu X, Ma Y, et al. (2020) Filling metal-organic framework mesopores with TiO_2 for CO_2 photoreduction. *Nature* 586: 549–554. http://doi.org/10.1038/s41586-020-2738-2
138. Loh JYY, Kherani NP, Ozin GA (2021) Persistent CO_2 photocatalysis for solar fuels in the dark. *Nat Sustain* 4: 466–473. https://doi.org/10.1038/s41893-021-00681-y
139. Gao W, Li S, He H, et al. (2021) Vacancy-defect modulated pathway of photoreduction of CO_2 on single atomically thin $AgInP_2S_6$ sheets into olefiant gas. *Nat Commun* 12: 4747. https://doi.org/10.1038/s41467-021-25068-7
140. Li K, Peng B, Peng T (2016) Recent advances in heterogeneous photocatalytic CO_2 conversion to solar fuels. *ACS Catal* 6: 7485–7527. http://doi.org/10.1021/acscatal.6b02089
141. Zhou M, Wang S, Yang P, et al. (2018) Boron carbon nitride semiconductors decorated with CdS nanoparticles for photocatalytic reduction of CO_2. *ACS Catal* 8: 4928–4936. https://doi.org/10.1021/acscatal.8b00104
142. Pang H, Meng X, Li P, et al. (2019) Cation vacancy-initiated CO_2 photoreduction over ZnS for efficient formate production. *ACS Energy Lett* 4: 1387–1393. https://doi.org/10.1021/acsenergylett.9b00711
143. Yang Z, Yang J, Ji H, et al. (2022) Construction of S–Co–S internal electron transport bridges in Co-doped $CuInS_2$ for enhancing photocatalytic CO_2 reduction. *Mater Today Chem* 26: 101078. https://doi.org/10.1016/j.mtchem.2022.101078

144. Kong Y, Li Y, Zhang Y, et al. (2021) Unveiling the selectivity of CO_2 reduction on Cu_2ZnSnS_4: The effect of exposed termination. *J Phys Chem C* 125: 24967–24973. https://doi.org/10.1021/acs.jpcc.1c08013
145. Yoshida T, Yamaguchi A, Umezawa N, et al. (2018) Photocatalytic CO_2 reduction using a pristine Cu_2ZnSnS_4 film electrode under visible light irradiation. *J Phys Chem C* 122: 21695–21702. https://doi.org/10.1021/acs.jpcc.8b04241
146. Zhou S, Sun K, Huang J, et al. (2021) Accelerating electron-transfer and tuning product selectivity through surficial vacancy engineering on CZTS/CdS for photoelectrochemical CO_2 reduction. *Small* 17: e2100496. https://doi.org/10.1002/smll.202100496
147. Sharma N, Das T, Kumar S, et al. (2019) Photocatalytic activation and reduction of CO_2 to CH_4 over single phase nano Cu_3SnS_4: Acombined experimental and theoretical study. *ACS Appl Energy Mater* 2: 5677–5685. https://doi.org/10.1021/acsaem.9b00813
148. Zhao H, Duan J, Zhang Z, et al. (2022) S-scheme heterojunction and defect site engineering on $Cu_xIn_5S_8$−$Cu_{2-y}Se$ for highly efficient photoreduction of CO_2 to methanol. *ChemCatChem* 14: e202101733. https://doi.org/10.1002/cctc.202101733
149. Lian S, Kodaimati MS, Dolzhnikov DS, et al. (2017) Powering a CO_2 reduction catalyst with visible light through multiple sub-picosecond electron transfers from a quantum dot. *J Am Chem Soc* 139: 8931–8938. http://doi.org/10.1021/jacs.7b03134
150. Wang L, Zhang Z, Guan R, et al. (2022) Synergistic CO_2 reduction and tetracycline degradation by CuInZnS-$Ti_3C_2T_x$ in one photoredox cycle. *Nano Res* 15: 8010–8018. https://doi.org/10.1007/s12274-022-4661-3
151. Cheruvathoor Poulose A, Zoppellaro G, Konidakis I, et al. (2022) Fast and selective reduction of nitroarenes under visible light with an earth-abundant plasmonic photocatalyst. *Nat Nanotechnol* 17: 485–492. https://doi.org/10.1038/s41565-022-01087-3
152. Zhou S, Sun K, Toe CY, et al. (2022) Engineering a kesterite-based photocathode for photoelectrochemical ammonia synthesis from NO_x reduction. *Adv Mater* 34: e2201670. https://doi.org/10.1002/adma.202201670
153. Xu X, Tang D, Cai J, et al. (2019) Heterogeneous activation of peroxymonocarbonate by chalcopyrite ($CuFeS_2$) for efficient degradation of 2,4-dichlorophenol in simulated groundwater. *Appl Catal B-Environ* 251: 273–282. https://doi.org/10.1016/j.apcatb.2019.03.080
154. Liu K, Cui R, Liu Z, et al. (2023) Fractional thermal reduction of $CuInS_2$ quantum dot-sensitized Bi_2MoO_6 hierarchical flowers on S-doped biochar for dual Z-scheme/Mott–Schottky heterojunction construction: A strategy for efficient photocatalytic biorefineries. *ACS Sustainable Chem Eng* 11: 5400–5407. https://doi.org/10.1021/acssuschemeng.2c06572
155. Zhang Y, Chen X, Ye Y, et al. (2023) Photocatalytic oxygen reduction reaction over copper-indium-sulfide modified polymeric carbon nitride S-scheme heterojunction photocatalyst. *J Catal* 419: 9–18. https://doi.org/10.1016/j.jcat.2023.01.021
156. Delekar SD, Dhodamani AG, More KV, et al. (2018) Structural and optical properties of nanocrystalline TiO_2 with multiwalled carbon nanotubes and its photovoltaic studies using Ru(II) sensitizers. *ACS Omega* 3:2743–2756. https://doi.org/10.1021/acsomega.7b01316
157. Patil MS, Deshmukh PS, Dhodamani GA, et al. (2017) Different strategies for modification of titanium dioxide as heterogeneous catalyst in chemical transformations. *Curr Org Chem* 21: 821–833. http://doi.org/10.2174/1385272820666161013151816

158. Hunge YM, Yadav AA, Kulkarni SB, et al. (2018) A multifunctional ZnO thin film based devices for photoelectrocatalytic degradation of terephthalic acid and CO_2 gas sensing applications. *Sens Actuators B Chem* 274: 1–9. https://doi.org/10.1016/j.snb.2018.07.117
159. Wei Z, Liang F, Liu Y, et al. (2017) Photoelectrocatalytic degradation of phenol-containing wastewater by TiO_2/g-C_3N_4 hybrid heterostructure thin film. *Appl Catal B-Environ* 201: 600–606. https://doi.org/10.1016/j.apcatb.2016.09.003
160. Semalti P, Sharma V, Sharma SN (2022) A solution-route processed multicomponent $Cu_2ZnSn(S_{1-x}Se_x)_4$ nanocrystals: A potential low-cost photocatalyst. *J Clean Prod* 365: 132750. https://doi.org/10.1016/j.jclepro.2022.132750
161. Zheng XL, Yang YJ, Liu YH, et al. (2022) Fundamentals and photocatalytic hydrogen evolution applications of quaternary chalcogenide semiconductor: Cu_2ZnSnS_4. *Rare Met* 41: 2153–2168. https://doi.org/10.1007/s12598-021-01955-2
162. Hunge YM, Yadav AA, Liu S, et al. (2019) Sonochemical synthesis of CZTS photocatalyst for photocatalytic degradation of phthalic acid. *Ultrason Sonochem* 56: 284–289. https://doi.org/10.1016/j.ultsonch.2019.04.003
163. Tan Y, Lin ZQ, Ren WH, et al. (2012) Facile solvothermal synthesis of Cu_2SnS_3 architectures and their visible-light-driven photocatalytic properties. *Mater Lett* 89: 240–242. https://doi.org/10.1016/j.matlet.2012.08.117
164. Kush P, Deori K, Kumar A, et al. (2015) Efficient hydrogen/oxygen evolution and photocatalytic dye degradation and reduction of aqueous Cr(vi) by surfactant free hydrophilic Cu_2ZnSnS_4 nanoparticles. *J Mater Chem A* 3: 8098–8106. http://doi.org/10.1039/C4TA06551D

AIMS Press